ACS APPLIED MATERIALS & INTERFACES

Research Article

www.acsami.org

Porous Au−Ag Alloy Particles Inlaid AgCl Membranes As Versatile Plasmonic Catalytic Interfaces with Simultaneous, in Situ SERS Monitoring

Qi Cao,[†,§,#] Kaiping Yuan,[†] Qinghe Liu,[†] Chongyun Liang,[‡] Xiang Wang,[§,//] Yi-Feng Cheng,[†] Qingqing Li,[†] Min Wang,[†] and Renchao Che*[,†]

[†]Laboratory of Advanced Materials, Department of Materials Science, Collaborative Innovation Center of Chemistry for Energy Materials, Fudan University, Shanghai 200438, People's Republic of China

[‡]Department of Chemistry, Fudan University, Shanghai 200433, People's Republic of China

[//]School of Materials Science and Engineering, Tianjin University, Tianjin 300072, People's Republic of China

[§]School of Engineering, The University of Tokyo, 7-3-1 Hongo, Bunkyo-ku, Tokyo 113-8656, Japan

[#]Institute of Ion Beam Physics and Materials Research, Helmholtz-Zentrum Dresden-Rossendorf, Bautzner Landstraße 400, 01328 Dresden, Germany

Supporting Information

ABSTRACT: We present a novel porous Au−Ag alloy particles inlaid AgCl membrane as plasmonic catalytic interfaces with real-time, in situ surface-enhanced Raman spectroscopy (SERS) monitoring. The Au−Ag alloy particles inlaid AgCl membranes were obtained via a facile two-step, air-exposed, and room-temperature immersion reaction with appropriate annealing process. Owing to the designed integration of semiconductor component AgCl and noble metal Au−Ag particles, both the catalytic reduction and visible-light-driven photocatalytic activities toward organic contaminants were attained. Specifically, the efficiencies of about 94% of 4-nitrophenol (4-NP, 5×10^{-5} M) reduction after 8 min of reaction, and degradation of rhodamine 6G (R6G, 10^{-5} M) after 12 min of visible light irradiation were demonstrated. Moreover, efficiencies of above 85% of conversion of 4-NP to 4-aminophenol (4-AP) and 90% of R6G degradation were achieved as well after 6 cycles of reactions, by which robust recyclability was confirmed. Further, with distinct SERS signals generated simultaneously from the surfaces of Au−Ag particles under laser excitation, in situ SERS monitoring of the process of catalytic reactions with superior sensitivity and linearity has been realized. Overall, the capability of the Au−Ag particles inlaid AgCl membranes to provide SERS monitored catalytic and visible-light-driven photocatalytic conversion of organic pollutants, along with their mild and cost-effective fabrication method, would make sense for in-depth understanding of the mechanisms of (photo)catalytic reactions, and also future development of potable, multifunctional and integrated catalytic and sensing devices.

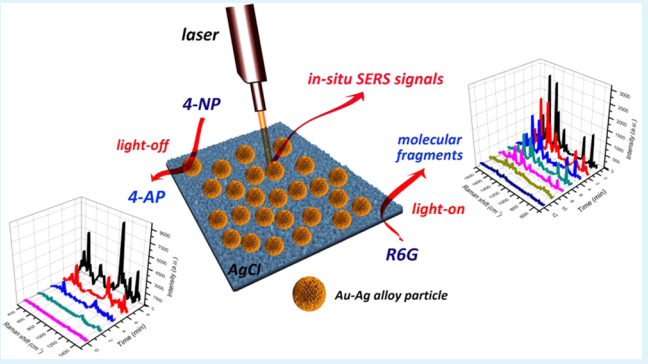

KEYWORDS: *Au−Ag alloy, SERS monitoring, catalysis, photocatalysis, persistent organic pollutants*

INTRODUCTION

Since the first Ag@AgCl plasmonic photocatalyst was proposed,[1] plasmonic catalytic materials have given rise to considerable interest.[2−5] Unlike conventional photocatalysts, plasmonic photocatalytic systems were generally obtained via designed integration of plasmonic noble metal components and semiconductors into a same system at micro- or nanoscale to achieve improved photophysical and photochemical properties. On one hand, regarding the semiconductor components, noble metal decorations may have the potentiality to enhance their photocatalytic efficiency and light-harvesting capability via several mechanisms. First, the surface plasmon resonance (SPR) effect of noble metal nanoparticles can help to capture a broader band of solar spectrum, and thereby achieve a higher utilization rate of solar energy. Second, the energy-level alignment in noble metal−semiconductor hybrids is favorable to electron injection from Fermi level of noble metals to the top of valence band of semiconducting components, bringing about more photogenerated electron/hole pairs as reducing/oxidizing agents for photocatalytic reactions. Besides, the introduction of noble metal units may also enhance photocatalytic efficiency by promoting the charge separation process

Received: May 31, 2015
Accepted: August 11, 2015
Published: August 11, 2015

DOI: 10.1021/acsami.5b04769
ACS Appl. Mater. Interfaces 2015, 7, 18491−18500

at metal−semiconductor interfaces. Metallic components, attributed to their better electron affinity, can serve as the electron sink to reserve photogenerated electrons from semiconductors, and therefore delay the charge recombination process at the surfaces of catalysts.[6−12]

On the other hand, another powerful spectroscopic technique based mainly on rough surfaces of noble metal nanostructures, the surface-enhanced Raman scattering (SERS) spectroscopy, has also been introduced into plasmonic photocatalytic systems recently, and so far triggered several promising applications like the photocatalytic degradation induced self-cleaning and recyclable SERS platforms,[13−16] or inversely, the in situ SERS monitoring of plasmon-enhanced catalytic reactions.[17−20] SERS spectroscopy, as a quite helpful tool for trace detection of organic contaminants with high sensitivity and rapid response,[21−23] exhibits great superiority over traditionally utilized nonsurface-selective UV−visible (UV−vis) absorption spectroscopy for monitoring catalytic reactions.[24,25] Since SERS spectra can provide real-time molecular-level vibrational information on specific functional groups, it is possible to acquire unique fingerprints of investigated molecules on the surfaces of catalysts up to single-molecule sensitivity and thus reveal the real mechanisms of catalytic reactions.[26] Therefore, the composites consisting of semiconductor photocatalysts and noble metal SERS platforms hold great potential to offer real-time and in situ SERS monitored catalytic reactions of organic pollutants, and hence are highly demanded for both mechanism investigations of catalytic reactions and environmental/health monitoring and management applications nowadays.

Here, in this work, we present a novel plasmonic catalytic Au−Ag alloy particles inlaid AgCl membrane prepared via a facile two-step wet immersion reaction accompanied by appropriate annealing process. The preparation method shows great advantages as the wet immersion reactions were directly conducted in air under room temperature and the annealing process was also a relatively low-temperature and rapid one (300 °C, 2 h). In addition, since silver has played a major role in noble metal elements of the Au−Ag alloy particles inlaid AgCl membranes, it is reasonable that they are more cost-effective than other traditional single- or multicomponent Au/Pt/Pd based catalytic systems.[27−29] Meanwhile, the semiconductor component AgCl also demonstrates superiority compared to the conventionally utilized oxides (e.g., TiO_2[17] and ZnO[18]) and sulfides (e.g., ZnS[30] and CdS[31]) photocatalysts which usually suffer a lot from intrinsic drawbacks of inferior chemical stability under acidic conditions and light irradiation (i.e., the photocorrosion problem).

Typically, it is owing to the successful integration of plasmonic noble metals gold and silver as well as semiconducting AgCl that complementary behaviors of real-time and in situ SERS monitoring of catalytic reduction and visible-light-driven photocatalytic degradation of model molecules 4-nitrophenol (4-NP) and rhodamine 6G (R6G) have been realized in this work. For one thing, as catalytic and photocatalytic platforms, the Au−Ag alloy particles inlaid AgCl membranes achieved not only superior efficiency but also appreciable recyclability, and it is also mentionable that thanks to the SPR of noble metals Au and Ag, the highly demanded photocatalytic activity driven by visible light has been achieved in the Au−Ag particles inlaid AgCl system. For another, it is ascribed to the intensively existing rough surfaces of porous Au−Ag alloy particles supported on AgCl membranes that simultaneous in situ SERS signals could generate and hence be recorded to monitor the process of catalytic reactions. Amazingly in this work, besides the high efficiency as well as stability of catalytic and photocatalytic reactions, also quite good linearity and sensitivity of in situ SERS monitoring have been achieved using the Au−Ag particles inlaid AgCl membranes, suggesting that monitoring catalytic processes with SERS technique is reliable indeed. Hence, it is believable that the Au−Ag alloy particles inlaid AgCl membranes demonstrated in this work, with their facile preparation and attractive catalytic, photocatalytic and SERS applications, may bring inspirations for future development of integrated multifunctional catalytic and detection devices.

RESULTS AND DISCUSSION

The Au−Ag particles inlaid AgCl membrane was prepared via an air-exposed, two-step wet immersion reaction at room temperature along with appropriate annealing process. First, Ag_3PO_4 membrane was first obtained on Ag foils according to a previous report.[32] Figure S1 displays representative XRD pattern, EDS spectrum, as well as SEM images of the on-chip membrane. With both the XRD and EDS results demonstrating the pure Ag_3PO_4 phase, it is obvious that the first-step immersion into the NaH_2PO_4 and H_2O_2 based mixture solution has achieved successful surface coating of Ag_3PO_4 onto pristine silver foils, and after the second-step immersion in the $HAuCl_4$ solution under specific pH condition, the PO_4^{3-} ions were displaced by Cl^- ions, and meanwhile the Au−Ag nanoparticles appeared as well. Afterward, particle aggregation occurred accompanied by the Ostwald ripening process during annealing,[33] finally generating Au−Ag alloy particles with their average size at micrometer scale.

Figures 1−2 demonstrate the phase components and morphologies of the eventually obtained Au−Ag particles inlaid AgCl membranes. The XRD pattern in Figure 1a reveals the coexistence of cubic phase AgCl (PDF#31-1238), Ag (PDF#04-0783), and Au (PDF#04-0784) with all characteristic diffraction peaks well identified and indexed. From the sharp shapes of characteristic peaks, it can be known that high crystallinity was achieved after the annealing process. In addition, it can be observed from the magnified XRD patterns of the (111), (200), and (220) crystal planes (Figure 1b) that the peak positions of the sample distinctively lie between the positions of pure Ag and pure Au phase, further revealing that Ag atoms and Au atoms have entered into each other's crystal lattices and thereby formed alloyed phase.[34] Besides, as shown in Figure S2, a distinct characteristic band corresponding to Ag−Cl stretching mode at 241 cm^{-1} in room-temperature Raman spectrum of the sample gives the spectroscopic evidence of the formation of AgCl phase as well.[35]

Figure 2 displays the representative SEM images and EDS profiles of the obtained composite membranes. It is obvious that discrete particles with porous nature and uniform size of about 15 μm can be observed all over the supporting membrane. The elemental analysis results of a single particle (Figure 2c and d), as well as the membrane only (Figure 2e and f) together indicate that the compositions of the particles and membrane were in fact Au−Ag alloys and pure AgCl respectively, which is also witnessed by EDS elemental mapping profiles exhibited in Figure S3. The approximate atom concentration ratio of Au and Ag in these alloy particles was 2:5 according to EDS results in Figure 2d. Nevertheless, although the EDS spectrum of Figure 2f tells that the

DOI: 10.1021/acsami.5b04769
ACS Appl. Mater. Interfaces 2015, 7, 18491−18500

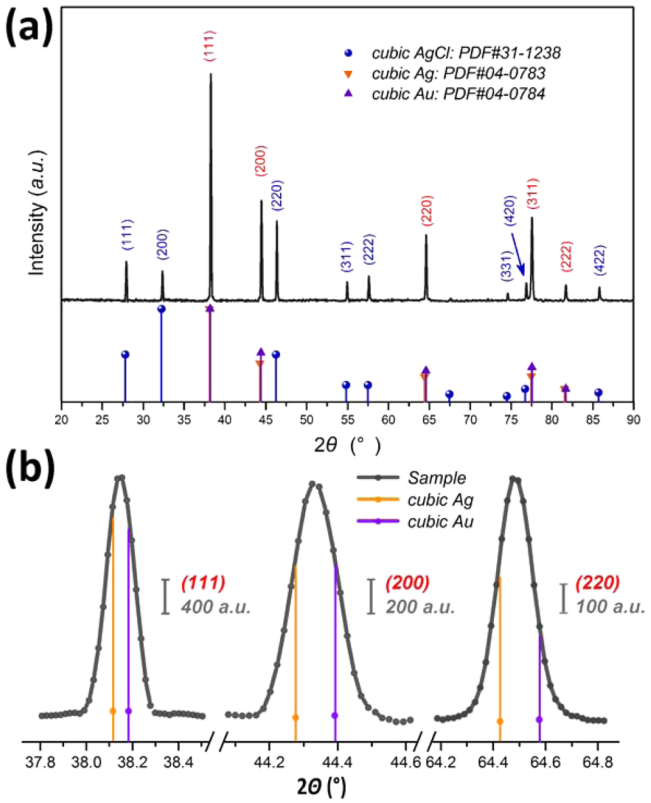

Figure 1. (a) Representative XRD pattern of the obtained Au−Ag alloy particles inlaid AgCl membrane. (b) Magnified images of the characteristic diffraction peaks ascribed to (111), (200), and (220) crystal planes of the Au−Ag alloy.

supporting membrane contained nothing but AgCl, it can be seen in SEM images of Figure 2b−c that there were in fact very small Au−Ag nanoparticles (i.e., the small white dots), which formed after immersion into $HAuCl_4$ aqueous solution but before annealing, distributing on the AgCl membrane, and it might be ascribed to their ultrasmall sizes compared to Au−Ag alloy microparticles and the consequent low content that no gold element has been detected in the EDS spectrum of Figure 2f. Besides, the large amount of carbon shown in EDS spectra of Figure 2d and f and oxygen in Figure 2d could be ascribed to the existence of polyvinylpyrrolidone (PVP) molecules and other organics used in previous immersion reactions since PVP is essentially stable at the temperature of 300 °C during annealing process.[36] It is notable as well that the macroporous nature of these Au−Ag alloy particles could also be clearly discerned from SEM images of Figure 2b and c and Figure S3a, reflecting the rationality for these Au−Ag alloy particles to have large and rough surfaces, and further have the chance to provide appreciable SERS signals and catalytic performance for reduction of 4-NP.

Figure 3 exhibits the TEM characterization results of the Au−Ag alloy particles. SAED pattern in Figure 3c, in which the distinct (111), (200), and (220) crystal planes could be observed, shows similar results with previous XRD analysis, confirming the formation of Au−Ag alloys inside each microparticle. It is clear from TEM and HRTEM images of Figure 3a and b that besides the above-mentioned macroporous structures, these Au−Ag alloy particles showed interconnected network-like morphology with intensively existing inside mesopores at nanometer scale, and the size of primary particles varied from several nanometers to several tens of nanometers. The average grain size of these primary Au−Ag particles calculated using the diffraction peak of (111) crystal plane in the XRD pattern of Figure 1 according to Debye−Scherrer Formula[37] was about 49.2 nm, by which the average size of inside primary Au−Ag nanoparticles can also be perceived.

Figure 4 displays the UV−vis−NIR DRS spectra of the on-chip membranes obtained before (i.e., Ag_3PO_4) and after $HAuCl_4$ immersion and annealing process (i.e., the Au−Ag alloy particles inlaid AgCl membrane). As can be seen, the Au−Ag particles inlaid AgCl membrane shows greatly enhanced light absorption properties in visible and NIR band compared to the Ag_3PO_4 membrane which is consistent with related literature reports,[1,38] demonstrating the strong potential for Au−Ag alloy particles inlaid AgCl membranes to serve as visible light or sunlight driven photocatalysts. On the basis of the above discussion of the size of primary Au−Ag nanoparticles and previous literature reports,[39,40] it can be inferred that the characteristic band at about 485 nm in DRS spectrum of the Au−Ag alloy particles inlaid AgCl membrane (Figure 4, gray curve) was originated from the SPR of primary Au−Ag nanoparticles because the characteristic SPR bands of pure Au and Ag nanoparticles generally appear at about 520 nm[39] and 390 nm,[40] respectively.

Figure 5 gives an schematic illustration of the dual-mode in situ SERS monitoring process when using the Au−Ag particles inlaid on-chip AgCl membranes for catalytic conversion of 4-NP to 4-aminophenol (4-AP), and for visible-light-driven photocatalytic degradation reaction of R6G. Typically in the catalysis mode (i.e., "light-off" mode), the Au−Ag alloy particles supported on the surfaces of AgCl can absorb and consequently reduce the investigated molecules 4-NP, while in the photocatalysis mode (i.e., "light-on" mode), the intrinsically wide-band gap semiconductor AgCl mediated by SPR of Au−Ag alloy particles can provide visible-light-driven photocatalytic activity toward degradation of organic pollutant R6G. In addition, with simultaneous laser excitation, sensitive in situ SERS signals can be recorded, as well for real-time monitoring of the process of (photo)catalytic reactions.

Figure 6 displays the results of the catalytic reduction reaction of 4-NP to 4-AP. The catalytic reduction of 4-NP to 4-AP in the presence of an excess amount of $NaBH_4$ has often been used as a model reaction to evaluate the catalytic performance of noble metal nanoparticles. The metal particles start the catalytic reduction by relaying electrons from the donor $BH4^-$ to the acceptor 4-NP on the adsorption of both reactants on the particles, leading to the production of amido derivatives 4-AP.[41−43] As shown in Figure 6a and Figure S4, the absorption band of pure 4-NP aqueous solution located at about 317 nm of wavelength, and after the addition of $NaBH_4$, it shifted to 400 nm of wavelength, and remained at the same place after the Au−Ag alloy particles inlaid AgCl membranes were further introduced into the reaction solution as catalysts, which is consistent with previous studies.[44,45] The green curve in Figure S4 clearly proves that the presence of $NaBH_4$ but absence of Au−Ag alloy particles inlaid AgCl membranes could not lead to the reduction of 4-NP. And with the catalysis of Au−Ag alloy particles inlaid AgCl membranes, it is obvious in Figure 6a that the intensities of absorption at 400 nm corresponding to 4-NP decreased significantly as the reaction proceeded, revealing that 4-NP had been gradually reduced to 4-AP. As shown in Figure 6b, the calculated first-run conversion efficiency after 8 min of the reaction was about 93.5%, and also

DOI: 10.1021/acsami.5b04769
ACS Appl. Mater. Interfaces 2015, 7, 18491−18500

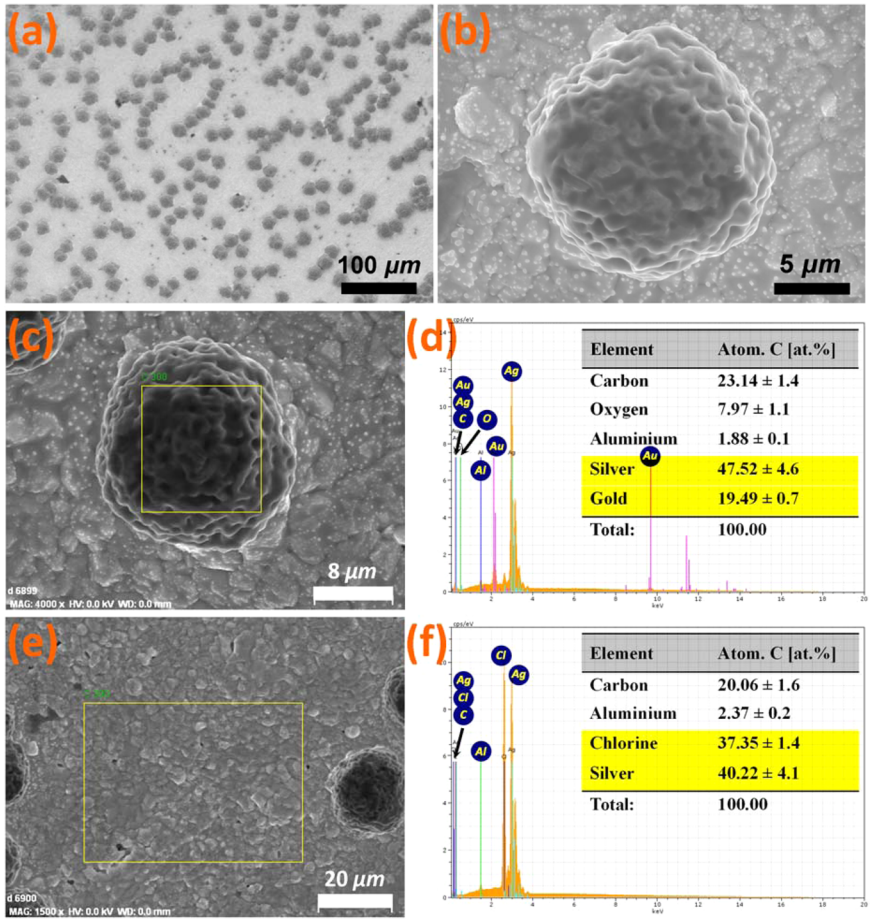

Figure 2. Representative (a and b) SEM images obtained at different magnifications of the obtained Au−Ag alloy particles inlaid AgCl membrane. (c and f) The SEM/EDS analysis of (c and d) a single Au−Ag alloy particle and (e and f) the AgCl membrane. The EDS spectra in panels d and f were collected from the selected areas labeled in panels c and e, respectively.

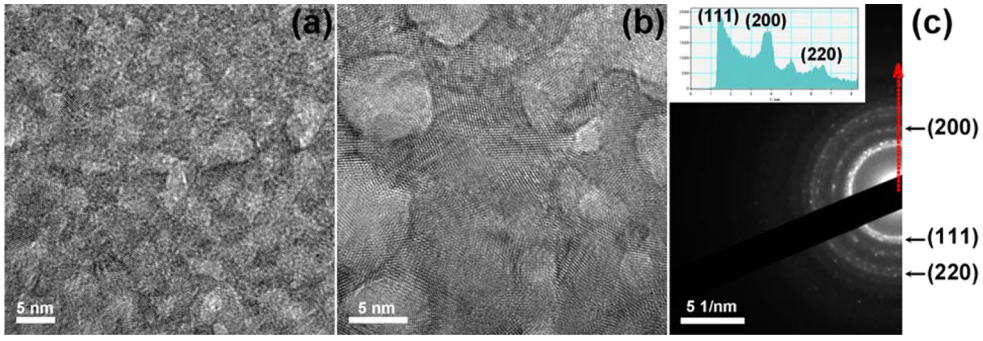

Figure 3. Representative (a) TEM image, (b) HRTEM image, as well as the (c) SAED pattern of the Au−Ag alloy particles. The inserted intensity line profile in panel (c) was recorded along the red arrowhead labeled in (c). The samples for TEM characterization were prepared by ultramicrotomy of the fragments of Au−Ag alloy particles obtained by continuous sonification.

a conversion efficiency of above 85% was still maintained after six cycles of the reactions, by which high efficiencies as well as superior durability and recyclability of the Au−Ag particles inlaid AgCl membranes as catalysts were confirmed. Overall, the high catalytic efficiency and recyclability can be attributed synergistically to the large effective surface areas of these Au−Ag alloy particles resulted from their unique hierarchical macro- and mesoporous structures as well as superior stability of the formed Au−Ag microparticles after aggregation and ripening process during calcining.

Figure 6c exhibits the in situ recorded SERS spectra from the porous surfaces of Au−Ag particles, revealing the dependence of the intensities of characteristic Raman scattering bands on reaction time. As can be seen, the spectrum recorded at $t = 0$ displays neglectable SERS signals due to the relatively weak interaction of 4-NP with the Au−Ag substrates. Nevertheless, when 4-NP was gradually transformed into 4-AP during the catalytic reaction, it was owing to the strong electrostatic bonding between amido groups of 4-AP and Au−Ag surfaces, and the derived strong electromagnetic interactions under laser excitation that the in situ SERS signals got increased obviously

DOI: 10.1021/acsami.5b04769
ACS Appl. Mater. Interfaces 2015, 7, 18491−18500

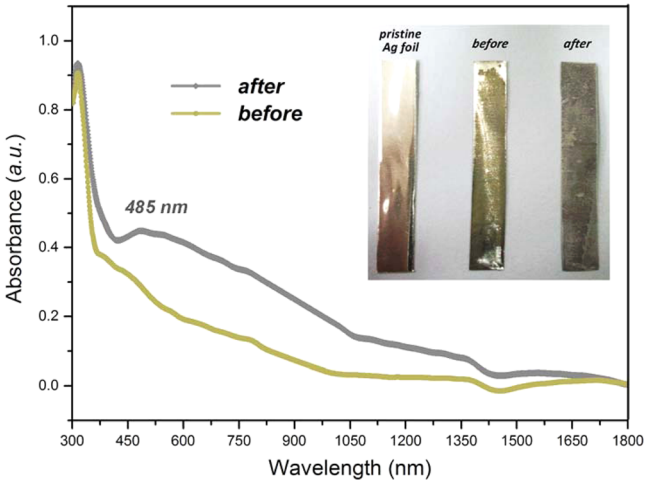

Figure 4. UV−vis−NIR diffusion reflectance spectra (DRS) of the on-chip membranes before (i.e., the Ag_3PO_4 membrane) and after immersion into $HAuCl_4$ aqueous solution and annealing (i.e., the Au−Ag alloy particles inlaid AgCl membrane). The inserted optical photograph shows the appearances of the two on-chip membranes, along with a piece of pristine silver foil.

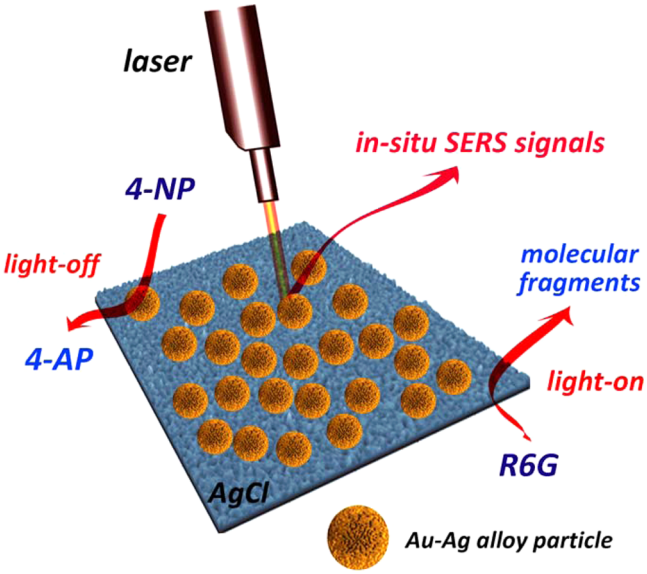

Figure 5. Schematic illustration of the dual-mode in situ SERS monitoring process for both the catalytic reduction reaction of 4-NP to 4-AP (i.e., "light-off" catalysis mode) and photocatalytic degradation reaction of R6G (i.e., "light-on" photocatalysis mode) using the plasmonic catalytic Au−Ag alloy particles inlaid AgCl membranes.

and thus can be easily detected. Notably, since the Au−Ag alloy particles supported on AgCl membranes acted as both catalytic active sites and SERS substrates, the reaction process could be monitored by observing the intensity variations of characteristic SERS bands during the catalytic reaction.[19]

As exhibited in Figure 6d, pseudo-first-order kinetic rate plots of the catalytic reactions were calculated, by which the rate constants and kinetics equations were also obtained, as summarized in Table 1. Unlike the case of UV−vis spectroscopic monitoring in which the gradually decreasing absorption intensities of 4-NP were used, the slopes of kinetics equations derived from SERS spectra are negative because the Raman bands of 4-AP gained higher intensities as the reaction proceeded. Considering that the reaction solution initially contained no 4-AP, here the band intensities recorded at t = 2 min were applied as initial references when calculating kinetic rate plots and kinetics equations via the time-dependent variation of in situ SERS signals. Particularly, the intensity variation of four specific characteristic SERS bands located at 492, 580, 1160, and 1424 cm^{-1} of Raman shift, which could be assigned to the stretching mode of C−C bond, in-plane bending mode of C−H bond, in-plane bending mode of C−O bond, and the mixed mode of both out-of-plane deformation and in-plane bending of C−C−C ring respectively,[46−48] were selected as models and identified carefully to investigate the process of catalytic reduction of 4-NP. As can be seen in Table 1, the slopes of kinetics equations (i.e., rate constants) calculated from SERS bands are essentially similar to each other within the range between −0.378 and −0.422. Moreover, the calculated Adj.-R^2 values of the curves, specifically, 0.9990 for the case of SERS characteristic band at 492 cm^{-1}, 0.9681 for 580 cm^{-1}, 0.9976 for 1160 cm^{-1}, and 0.9733 for 1424 cm^{-1}, all turns out to be much better than 0.9563 which was calculated via UV−vis absorbance spectra, demonstrating the superior linearity and stability when utilizing in situ SERS signals for monitoring the process of catalytic reduction of 4-NP to 4-AP.

Meanwhile, thanks to the plasmon-enhanced photocatalytic activity of semiconducting AgCl under visible light irradiation, the Au−Ag particles inlaid AgCl membranes could also be used for visible-light-driven photocatalytic degradation of organic contaminants. Here, we chose R6G as the model molecule. Similar to the catalytic reaction of 4-NP, the irradiation time-dependent UV−vis absorbance spectra and the results of recyclability test were displayed in Figure 7a and b. It is evident that nearly complete degradation of R6G molecules in 10^{-5} M aqueous solution was achieved. The degradation efficiency after 12 min of visible light irradiation during the first and sixth cycle of photocatalytic reaction was calculated to be 93.4% and 90.7%, respectively, revealing the relatively high, stable, and long-lived visible-light-driven photocatalytic activity of the Au−Ag alloy particles inlaid AgCl membranes toward R6G degradation. As has been discussed in Introduction section, the considerable visible-light-driven photocatalytic efficiency might be derived from not only the charge transfer process induced by band alignment effects as well as efficient exciton−plasmon interactions, but also the charge separation process between photogenerated electron/hole pairs because of the better electron affinity of Au−Ag alloy particles than semiconducting AgCl.[8−10,49] As a typical wide-band gap semiconductor, AgCl has a direct band gap of 5.6 eV. However, grains of AgCl are photosensitive due to their point ionic defects and electron traps. It is meaningful to consider how the Au−Ag alloy particles inlaid AgCl membrane became an efficient photocatalyst under visible light irradiation. The surface of AgCl is most likely to be terminated by Cl^-, and is therefore negatively charged. The primary Au−Ag nanoparticles on the surface of AgCl could separate its electron/hole distribution. Figure 4 has clearly demonstrated that the SPR band of these primary Au−Ag alloy nanoparticles could help the composite membranes absorb visible light, and in consideration of the dipolar character of the SPR of Au−Ag nanoparticles, the absorbed photons would be separated into electrons and holes efficiently and afterward distributed near the surfaces of Au−Ag nanoparticles and AgCl membranes, respectively. Finally, the holes on AgCl surfaces led to the

DOI: 10.1021/acsami.5b04769
ACS Appl. Mater. Interfaces 2015, 7, 18491−18500

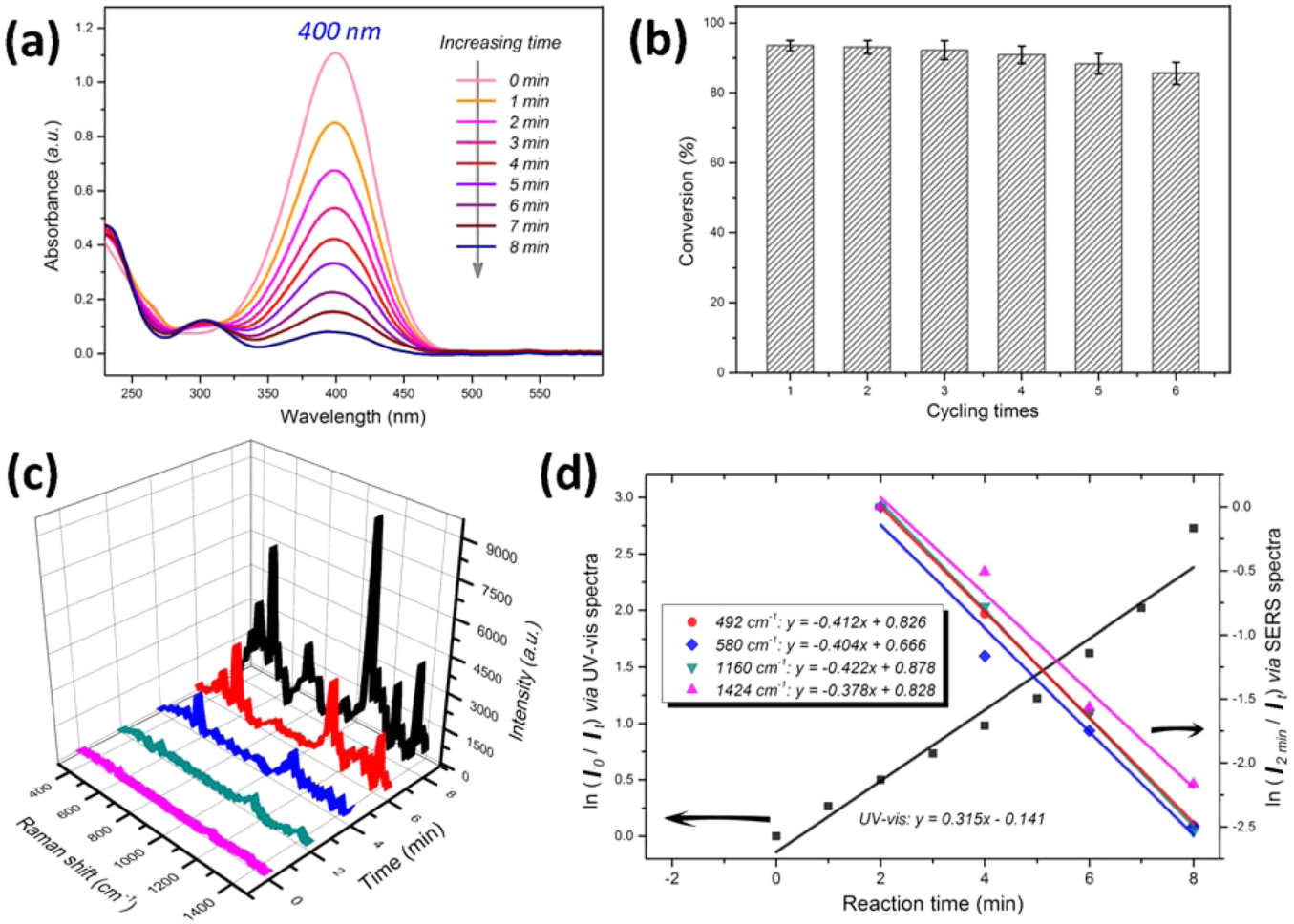

Figure 6. In-situ monitoring of catalytic reduction of 4-NP (5×10^{-5} M aqueous solution) to 4-AP: (a) time-dependent UV−vis absorbance spectra and (b) results of recyclability test. (c) In-situ SERS spectra recorded at different time points of the catalytic reaction along with (d) the pseudo-first-order kinetic rate plots and correspondingly fitted kinetics equations of the catalytic reaction in the presence of the Au−Ag alloy particles inlaid AgCl membranes. I_0, I_t, and I_{2min} in panel d represent the initial peak intensity at 400 nm of UV−vis spectra, the intensities of characteristic UV−vis absorbance or SERS bands at the time point of t, and the characteristic band intensities in the in situ SERS spectra after 2 min of the catalytic reduction reaction.

Table 1. Summary for the Fitted Pseudo-First-Order Kinetic Rate Constants (k), Kinetics Equations, and the Corresponding Adjusted Regression Coefficients (Adj.-R^2) for Catalytic Reduction Reaction of 4-NP to 4-AP Calculated Using the UV−vis Absorbance Band at 400 nm and Different Characteristic Bands Observed in In Situ SERS Spectra

method	characteristic band position	k (min^{-1})	Adj.-R^2	kinetics equation
UV−vis	400 nm	0.315	0.95630	$y = 0.315x - 0.141$
SERS	492 cm^{-1}	−0.412	0.99904	$y = -0.412x + 0.826$
	580 cm^{-1}	−0.404	0.96810	$y = -0.404x + 0.666$
	1160 cm^{-1}	−0.422	0.99761	$y = -0.422x + 0.878$
	1424 cm^{-1}	−0.378	0.97328	$y = -0.378x + 0.828$

oxidation of Cl^- to Cl atoms, by which R6G molecules could be easily oxidized.[1,3]

On the other hand, the SPR effect, especially the plasmon resonance confined in local areas of rough and porous surfaces (i.e., localized surface plasmon resonance, LSPR) of the Au−Ag alloy particles had not only brought about enhanced photocatalytic reactivity for AgCl under visible light irradiation, but also offered large amount of electromagnetic "hot spots" under laser excitation,[50] and thereby generated in situ SERS signals for monitoring the reactions. As shown in the in situ SERS spectra obtained at different time points of the photocatalytic degradation reaction (Figure 7c), as well as correspondingly calculated pseudo-first-order kinetic rate plots and kinetics equations of the reactions (Figure 7d), characteristic SERS bands of R6G deteriorated gradually as the reaction proceeded, and after reaction for 12 min, the previously distinct SERS signals could be hardly identified any more, which could be regarded as the evidence of the degradation of R6G into small molecular fragments as well.

Typically, six characteristic Raman bands in SERS spectra corresponding respectively to the in-plane bending mode of C−C−C ring (611 cm^{-1}), out-of-plane bending motion of the hydrogen atoms of the xanthene skeleton (772 cm^{-1}), stretching vibration mode of the C−C bond (1184 cm^{-1}), and the aromatic C−C stretching vibration mode of R6G molecules (1360, 1508, and 1650 cm^{-1}),[26] were studied and exploited for monitoring the photocatalytic degradation process. As labeled in Figure 7d and summarized in Table 2, it is clear that all kinetics equations possess similar rate constants of about 0.200 ± 0.017. Furthermore, it can be known that the curve fitted via the kinetic rate plots obtained

DOI: 10.1021/acsami.5b04769
ACS Appl. Mater. Interfaces 2015, 7, 18491−18500

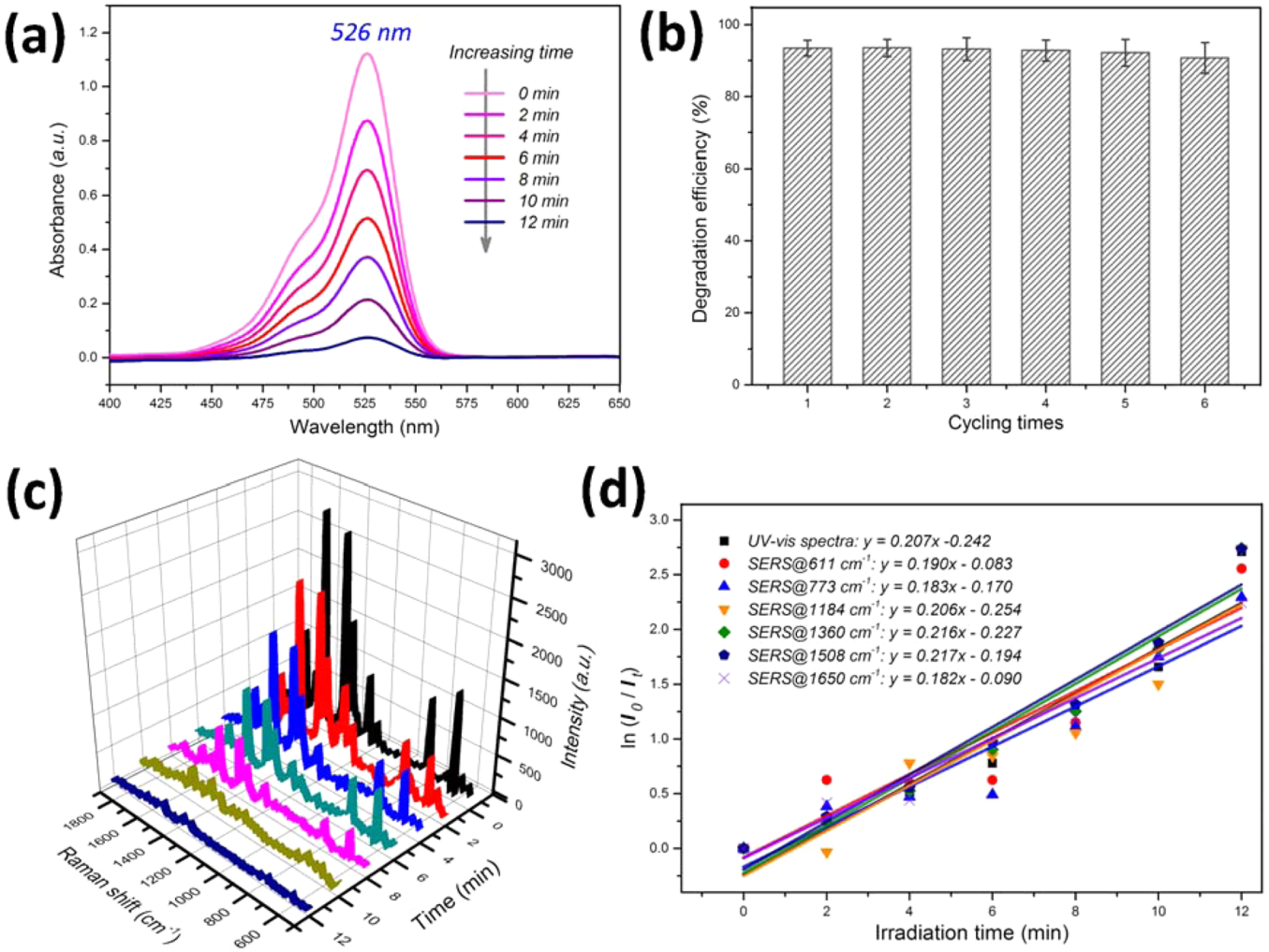

Figure 7. In situ monitoring of photocatalytic degradation reaction of R6G molecules in 10^{-5} M aqueous solution: (a) time-dependent UV−vis absorbance spectra and (b) results of the recyclability test. (c) In situ SERS spectra recorded at different time points of the photocatalytic degradation reaction and (d) the pseudo-first-order kinetic rate plots and correspondingly fitted kinetics equations of the reaction in the presence of Au−Ag alloy particles inlaid AgCl membranes. I_0 and I_t in panel (d) represent the peak intensities of the UV−vis absorbance spectra at 526 nm, or intensities of different characteristic bands in in situ SERS spectra, at the time point of $t = 0$ or t during the visible-light-driven photocatalytic R6G degradation reaction.

Table 2. Summary for the Fitted Pseudo-First-Order Kinetic Rate Constants (k), Kinetics Equations, as Well as the Corresponding Adjusted Regression Coefficients (Adj.-R^2) for the Photocatalytic Degradation Reaction of R6G Aqueous Solution Calculated via the UV−vis Absorbance Band at 526 nm and Different Characteristic Bands Observed in the in Situ SERS Spectra

method	characteristic band position	k (min^{-1})	Adj.-iR^2	kinetics equation
UV−vis	526 nm	0.207	0.89304	$y = 0.207x - 0.242$
SERS	611 cm^{-1}	0.190	0.86387	$y = 0.190x - 0.083$
	773 cm^{-1}	0.183	0.89119	$y = 0.183x - 0.170$
	1184 cm^{-1}	0.206	0.8573	$y = 0.206x - 0.254$
	1360 cm^{-1}	0.216	0.93329	$y = 0.216x - 0.227$
	1508 cm^{-1}	0.217	0.94791	$y = 0.217x - 0.194$
	1650 cm^{-1}	0.182	0.96155	$y = 0.182x - 0.090$

from UV−vis absorbance spectra turns out to have a relatively low *Adj.-R^2* value of 0.8930, while most of the other Adj.-R^2 values calculated from characteristic SERS bands are much higher, for example, 0.9616 calculated from the Raman band at 1650 cm^{-1}, and 0.9479 calculated from the Raman band at 1508 cm^{-1}. Therefore, it is believable that the stable rate constants, high Adj.-R^2 values, as well as good linearity of the in situ SERS monitoring technique could help to promote the accuracy and reliability for monitoring a variety of different catalytic and photocatalytic reactions.

To further investigate the sensitivity of the Au−Ag alloy particles inlaid AgCl membranes as SERS substrates for trace detection of organic contaminants, the limit of detection (LOD) toward the widely used SERS model molecules, that is, 4-aminothiophenol (4-ABT) molecules has also been studied, as demonstrated in Figure S5. Obviously, the distinct characteristic SERS bands at about 1078, 1142, 1184, 1389, 1432, and 1588 cm^{-1} of 4-ABT could be identified and agree well with literature values.[51] Particularly, it can be observed that although the concentration of the dilute solution of 4-ABT reached as low as 10^{-12} M, still several characteristic SERS bands could be discerned in the green curve (curve *v*), indicating that the AgCl supported Au−Ag substrate has achieved a quite appreciable LOD (10^{-12} M) for 4-ABT, which

DOI: 10.1021/acsami.5b04769
ACS Appl. Mater. Interfaces 2015, 7, 18491−18500

might be enabled by the readily formed chemical bonding between thiolate molecules and Au−Ag substrates, as well as moderate sizes of primary Au−Ag nanoparticles.[52] Furthermore, as described in the Supporting Information, the Raman enhancement factor (EF) of the composite substrate calculated using the 10^{-4} M 4-ABT case turns out to be 1.74×10^5, which also demonstrates the high sensitivity for SERS detection achieved by the Au−Ag alloy particles inlaid AgCl membranes. On the other hand, SEM images of the Au−Ag particles inlaid AgCl membranes were recorded after experiencing the SERS monitored (photo)catalytic reactions (Figure S6), confirming that no significant morphological changes occurred, and hence the composite membranes were essentially stable in spite of the continuous light irradiation and heating effect of Raman laser during the SERS monitoring process. The reliable chemical stability of the composite membrane might be originated from their micrometer sizes as well as hierarchically porous structures, and consequently contributed to the appreciable retention of catalytic efficiencies during the above-mentioned recyclability tests. All of these together prove that the Au−Ag alloy particles inlaid AgCl membranes presented in this work are indeed capable candidates for stable (photo)catalytic platforms allowing sensitive in situ SERS monitoring.

CONCLUSIONS

In summary, the novel porous Au−Ag alloy particles inlaid AgCl on-chip membranes prepared via a facile immersion reaction and annealing process were demonstrated for the first time as versatile plasmonic catalytic interfaces allowing simultaneous, in situ SERS monitoring. Thanks to the successful integration of noble metal Au−Ag particles and semiconductor AgCl, high efficiencies and robust recyclability of catalytic reduction of 4-NP to 4-AP and plasmon-enhanced visible-light-driven photocatalytic degradation of R6G were achieved. Meanwhile, the porous surfaces of Au−Ag alloy particles also generated sensitive in situ SERS signals simultaneously under laser excitation, using which the real-time monitoring of (photo)catalytic reactions could also be realized. To conclude, it is quite believable that the integration of catalytic and visible-light-driven photocatalytic activities with real-time and in situ SERS monitoring on the novel Au−Ag alloy particles inlaid AgCl membranes, along with their facile, mild and cost-effective preparation method, would not only help to understand the mechanisms of different catalytic reactions, but also bring inspirations for future development of novel potable, integrated and multifunctional catalytic and sensing devices.

ASSOCIATED CONTENT

Supporting Information

The Supporting Information is available free of charge on the ACS Publications website at DOI: 10.1021/acsami.5b04769.

Experimental details and supporting Figures S1−S7 (PDF)

AUTHOR INFORMATION

Corresponding Author

*E-mail: rcche@fudan.edu.cn.

Notes

The authors declare no competing financial interest.

ACKNOWLEDGMENTS

This work was supported by the Ministry of Science and Technology of China (973 Project No. 2013CB932901), and the National Natural Foundation of China (Nos. 11274066, 51172047, 51102050, U1330118). This project was sponsored by Shanghai Pujiang Program and "Shu Guang" project of Shanghai Municipal Education Commission and Shanghai Education Development Foundation (09SG01). Q. Cao acknowledges the support of Helmholtz-Zentrum Dresden-Rossendorf Summer Student Program Research Grant and China Scholarship Council (No. 201506100018).

REFERENCES

(1) Wang, P.; Huang, B. B.; Qin, X. Y.; Zhang, X. Y.; Dai, Y.; Wei, J. Y.; Whangbo, M. H. Ag@AgCl: A Highly Efficient and Stable Photocatalyst Active under Visible Light. *Angew. Chem., Int. Ed.* **2008**, *47*, 7931−7933.

(2) Pincella, F.; Isozaki, K.; Miki, K. A Visible Light-Driven Plasmonic Photocatalyst. *Light: Sci. Appl.* **2014**, *3*, e133.

(3) Hu, C.; Peng, T. W.; Hu, X. X.; Nie, Y. L.; Zhou, X. F.; Qu, J. H.; He, H. Plasmon-Induced Photodegradation of Toxic Pollutants with Ag−AgI/Al_2O_3 under Visible-Light Irradiation. *J. Am. Chem. Soc.* **2010**, *132*, 857−862.

(4) Awazu, K.; Fujimaki, M.; Rockstuhl, C.; Tominaga, J.; Murakami, H.; Ohki, Y.; Yoshida, N.; Watanabe, T. A Plasmonic Photocatalyst Consisting of Silver Nanoparticles Embedded in Titanium Dioxide. *J. Am. Chem. Soc.* **2008**, *130*, 1676−1680.

(5) Chen, X.; Zhu, H. Y.; Zhao, J. C.; Zheng, Z. T.; Gao, X. P. Visible-Light-Driven Oxidation of Organic Contaminants in Air with Gold Nanoparticle Catalysts on Oxide Supports. *Angew. Chem., Int. Ed.* **2008**, *47*, 5353−5356.

(6) Yin, Z. Y.; Wang, Z.; Du, Y. P.; Qi, X. Y.; Huang, Y. Z.; Xue, C.; Zhang, H. Full Solution-Processed Synthesis of All Metal Oxide-Based Tree-like Heterostructures on Fluorine-Doped Tin Oxide for Water Splitting. *Adv. Mater.* **2012**, *24*, 5374−5378.

(7) Li, P.; Wei, Z.; Wu, T.; Peng, Q.; Li, Y. D. Au−ZnO Hybrid Nanopyramids and Their Photocatalytic Properties. *J. Am. Chem. Soc.* **2011**, *133*, 5660−5663.

(8) Cao, Q.; Che, R. C. Tailoring Au−Ag−S Composite Microstructures in One-Pot for Both SERS Detection and Photocatalytic Degradation of Plasticizers DEHA and DEHP. *ACS Appl. Mater. Interfaces* **2014**, *6*, 7020−7027.

(9) Cao, S. W.; Yin, Z.; Barber, J.; Boey, F. Y. C.; Loo, S. C. J.; Xue, C. Preparation of Au−$BiVO_4$ Heterogeneous Nanostructures as Highly Efficient Visible-Light Photocatalysts. *ACS Appl. Mater. Interfaces* **2012**, *4*, 418−423.

(10) Li, M.; Yu, X. F.; Liang, S.; Peng, X. N.; Yang, Z. J.; Wang, Y. L.; Wang, Q. Q. Synthesis of Au−CdS Core−Shell Hetero-Nanorods with Efficient Exciton−Plasmon Interactions. *Adv. Funct. Mater.* **2011**, *21*, 1788−1794.

(11) Qi, X. Y.; Xue, C.; Huang, X.; Huang, Y. Z.; Zhou, X. Z.; Li, H.; Liu, D. J.; Boey, F.; Yan, Q. Y.; Huang, W.; De Feyter, S.; Muellen, K.; Zhang, H. Polyphenylene Dendrimer-Templated *In−Situ* Construction of Inorganic−Organic Hybrid Rice-Shaped Architectures. *Adv. Funct. Mater.* **2010**, *20*, 43−49.

(12) Liu, N. G.; Prall, B. S.; Klimov, V. I. Hybrid Gold/Silica/Nanocrystal-Quantum-Dot Superstructures: Synthesis and Analysis of Semiconductor-Metal Interactions. *J. Am. Chem. Soc.* **2006**, *128*, 15362−15363.

(13) Zou, X. X.; Silva, R.; Huang, X. X.; Al-Sharab, J. F.; Asefa, T. A Self-Cleaning Porous TiO_2−Ag Core-Shell Nanocomposite Material for Surface-Enhanced Raman Scattering. *Chem. Commun.* **2013**, *49*, 382−384.

(14) Lin, Y.; Bunker, C. E.; Fernando, K. A. S.; Connell, J. W. Aqueously Dispersed Silver Nanoparticle-Decorated Boron Nitride Nanosheets for Reusable, Thermal Oxidation-Resistant Surface

DOI: 10.1021/acsami.5b04769
ACS Appl. Mater. Interfaces 2015, 7, 18491−18500

Enhanced Raman Spectroscopy (SERS) Devices. *ACS Appl. Mater. Interfaces* **2012**, *4*, 1110−1117.
(15) Li, X. L.; Hu, H. L.; Li, D. H.; Shen, Z. X.; Xiong, Q. H.; Li, S. Z.; Fan, H. J. Ordered Array of Gold Semishells on TiO_2 Spheres: An Ultrasensitive and Recyclable SERS Substrate. *ACS Appl. Mater. Interfaces* **2012**, *4*, 2180−2185.
(16) Cao, Q.; Che, R. C.; Chen, N. Facile and Rapid Growth of Ag_2S Microrod Arrays as Efficient Substrates for Both SERS Detection and Photocatalytic Degradation of Organic Dyes. *Chem. Commun.* **2014**, *50*, 4931−4933.
(17) Salmistraro, M.; Schwartzberg, A.; Bao, W.; Depero, L. E.; Weber-Bargioni, A.; Cabrini, S.; Alessandri, I. Triggering and Monitoring Plasmon-Enhanced Reactions by Optical Nanoantennas Coupled to Photocatalytic Beads. *Small* **2013**, *9*, 3301−3307.
(18) Wen, C. Y.; Liao, F.; Liu, S. S.; Zhao, Y.; Kang, Z. H.; Zhang, X. L.; Shao, M. W. Bi-functional ZnO−RGO−Au Substrate: Photocatalysts for Degrading Pollutants and SERS Substrates for Real-Time Monitoring. *Chem. Commun.* **2013**, *49*, 3049−3051.
(19) Xu, B. B.; Zhang, R.; Liu, X. Q.; Wang, H.; Zhang, Y. L.; Jiang, H. B.; Wang, L.; Ma, Z. C.; Ku, J. F.; Xiao, F. H.; Sun, H. B. On-Chip Fabrication of Silver Microflower Arrays as a Catalytic Microreactor for Allowing *in situ* SERS Monitoring. *Chem. Commun.* **2012**, *48*, 1680−1682.
(20) Xu, B. B.; Zhang, Y. L.; Wei, S.; Ding, H.; Sun, H. B. On-Chip Catalytic Microreactors for Modern Catalysis Research. *ChemCatChem* **2013**, *5*, 2091−2099.
(21) Porter, M. D.; Lipert, R. J.; Siperko, L. M.; Wang, G. F.; Narayanan, R. SERS as a Bioassay Platform: Fundamentals, Design, and Applications. *Chem. Soc. Rev.* **2008**, *37*, 1001−1011.
(22) Nie, S. M.; Emery, S. R. Probing Single Molecules and Single Nanoparticles by Surface-Enhanced Raman Scattering. *Science* **1997**, *275*, 1102−1106.
(23) Xie, W.; Walkenfort, B.; Schlucker, S. Label-Free SERS Monitoring of Chemical Reactions Catalyzed by Small Gold Nanoparticles Using 3D Plasmonic Superstructures. *J. Am. Chem. Soc.* **2013**, *135*, 1657−1660.
(24) Zhou, W. J.; Liu, H.; Wang, J. Y.; Liu, D.; Du, G. J.; Cui, J. J. Ag_2O/TiO_2 Nanobelts Heterostructure with Enhanced Ultraviolet and Visible Photocatalytic Activity. *ACS Appl. Mater. Interfaces* **2010**, *2*, 2385−2392.
(25) Li, Y. Z.; Zhang, H.; Guo, Z. M.; Han, J. J.; Zhao, X. J.; Zhao, Q. N.; Kim, S. J. Highly Efficient Visible-Light-Induced Photocatalytic Activity of Nanostructured AgI/TiO_2 Photocatalyst. *Langmuir* **2008**, *24*, 8351−8357.
(26) Zhao, X. M.; Zhang, B. H.; Ai, K. L.; Zhang, G.; Cao, L. Y.; Liu, X. J.; Sun, H. M.; Wang, H. S.; Lu, L. H. Monitoring Catalytic Degradation of Dye Molecules on Silver-Coated ZnO Nanowire Arrays by Surface-Enhanced Raman Spectroscopy. *J. Mater. Chem.* **2009**, *19*, 5547−5553.
(27) Fang, P. P.; Duan, S.; Lin, X. D.; Anema, J. R.; Li, J. F.; Buriez, O.; Ding, Y.; Fan, F. R.; Wu, D. Y.; Ren, B.; Wang, Z. L.; Amatore, C.; Tian, Z. Q. Tailoring Au-Core Pd-Shell Pt-Cluster Nanoparticles for Enhanced Electrocatalytic Activity. *Chem. Sci.* **2011**, *2*, 531−539.
(28) Zheng, J. M.; Dong, Y. L.; Wang, W. F.; Ma, Y. H.; Hu, J.; Chen, X. J.; Chen, X. G. *In Situ* Loading of Gold Nanoparticles on Fe_3O_4@SiO_2 Magnetic Nanocomposites and Their High Catalytic Activity. *Nanoscale* **2013**, *5*, 4894−4901.
(29) Hu, W. T.; Liu, B. C.; Wang, Q.; Liu, Y.; Liu, Y. X.; Jing, P.; Yu, S. L.; Liu, L. X.; Zhang, J. A Magnetic Double-Shell Microsphere as a Highly Efficient Reusable Catalyst for Catalytic Applications. *Chem. Commun.* **2013**, *49*, 7596−7598.
(30) Sun, Y. F.; Sun, Z. H.; Gao, S.; Cheng, H.; Liu, Q. H.; Piao, J. Y.; Yao, T.; Wu, C. Z.; Hu, S. L.; Wei, S. Q.; Xie, Y. Fabrication of Flexible and Freestanding Zinc Chalcogenide Single Layers. *Nat. Commun.* **2012**, *3*, 1057.
(31) Xu, Y.; Zhao, W. W.; Xu, R.; Shi, Y. M.; Zhang, B. Synthesis of Ultrathin CdS Nanosheets as Efficient Visible-Light-Driven Water Splitting Photocatalysts for Hydrogen Evolution. *Chem. Commun.* **2013**, *49*, 9803−9805.
(32) Hu, H. Y.; Jiao, Z. B.; Yu, H. C.; Lu, G. X.; Ye, J. H.; Bi, Y. P. Facile Synthesis of Tetrahedral Ag_3PO_4 Submicro-Crystals with Enhanced Photocatalytic Properties. *J. Mater. Chem. A* **2013**, *1*, 2387−2390.
(33) Qin, G. W.; Liu, J. C.; Balaji, T.; Xu, X. N.; Matsunaga, H.; Hakuta, Y.; Zuo, L.; Raveendran, P. A Facile and Template-Free Method to Prepare Mesoporous Gold Sponge and Its Pore Size. *J. Phys. Chem. C* **2008**, *112*, 10352−10358.
(34) Liu, Q. H.; Cao, Q.; Zhao, X. B.; Bi, H.; Wang, C.; Wu, D. S.; Che, R. C. Insights into Size-Dominant Magnetic Microwave Absorption Properties of CoNi Microflowers *via* Off-Axis Electron Holography. *ACS Appl. Mater. Interfaces* **2015**, *7*, 4233−4240.
(35) Guerrini, L.; Garcia-Ramos, J. V.; Domingo, C.; Sanchez-Cortes, S. Nanosensors Based on Viologen Functionalized Silver Nanoparticles: Few Molecules Surface-Enhanced Raman Spectroscopy Detection of Polycyclic Aromatic Hydrocarbons in Interparticle Hot Spots. *Anal. Chem.* **2009**, *81*, 1418−1425.
(36) Du, Y. K.; Yang, P.; Mou, Z. G.; Hua, N. P.; Jiang, L. Thermal Decomposition Behaviors of PVP Coated on Platinum Nanoparticles. *J. Appl. Polym. Sci.* **2006**, *99*, 23−26.
(37) Cao, Q.; Liu, Z. W.; Che, R. C. Ordered Mesoporous $CoFe_2O_4$ Nanoparticles: Molten-Salt Assisted Rapid Nanocasting Synthesis and the Effects of Calcining Heating Rate. *New J. Chem.* **2014**, *38*, 3193−3198.
(38) An, C. H.; Peng, S.; Sun, Y. G. Facile Synthesis of Sunlight-Driven AgCl:Ag Plasmonic Nanophotocatalyst. *Adv. Mater.* **2010**, *22*, 2570−2574.
(39) Eustis, S.; El-Sayed, M. A. Why Gold Nanoparticles Are More Precious Than Pretty Gold: Noble Metal Surface Plasmon Resonance and Its Enhancement of the Radiative and Nonradiative Properties of Nanocrystals of Different Shapes. *Chem. Soc. Rev.* **2006**, *35*, 209−217.
(40) Jain, P. K.; Huang, X. H.; El-Sayed, I. H.; El-Sayed, M. A. Noble Metals on the Nanoscale: Optical and Photothermal Properties and Some Applications in Imaging, Sensing, Biology, and Medicine. *Acc. Chem. Res.* **2008**, *41*, 1578−1586.
(41) Li, J.; Liu, C. Y.; Liu, Y. Au/GrapheneHydrogel: Synthesis, Characterization and Its Use for Catalytic Reduction of 4-Nitrophenol. *J. Mater. Chem.* **2012**, *22*, 8426−8430.
(42) Zeng, J.; Zhang, Q.; Chen, J. Y.; Xia, Y. N. A Comparison Study of the Catalytic Properties of Au-Based Nanocages, Nanoboxes, and Nanoparticles. *Nano Lett.* **2010**, *10*, 30−35.
(43) Lin, F. H.; Doong, R. A. Bifunctional Au−Fe_3O_4 Heterostructures for Magnetically Recyclable Catalysis of Nitrophenol Reduction. *J. Phys. Chem. C* **2011**, *115*, 6591−6598.
(44) Chen, J. C.; Zhang, R. Y.; Han, L.; Tu, B.; Zhao, D. Y. One-Pot Synthesis of Thermally Stable Gold@Mesoporous Silica Core−Shell Nanospheres with Catalytic Activity. *Nano Res.* **2013**, *6*, 871−879.
(45) An, Q.; Yu, M.; Zhang, Y. T.; Ma, W. F.; Guo, J.; Wang, C. C. Fe_3O_4@Carbon Microsphere Supported Ag−Au Bimetallic Nanocrystals with the Enhanced Catalytic Activity and Selectivity for the Reduction of Nitroaromatic Compounds. *J. Phys. Chem. C* **2012**, *116*, 22432−22440.
(46) Philip, D.; John, A.; Panicker, C. Y.; Varghese, H. T. FT-Raman, FT-IR and Surface Enhanced Raman Scattering Spectra of Sodium Salicylate. *Spectrochim. Acta, Part A* **2001**, *57*, 1561−1566.
(47) Panicker, C. Y.; Varghese, H. T.; John, A.; Philip, D.; Istvan, K.; Keresztury, G. FT-IR, FT-Raman and FT-SERS Spectra of 4-Aminosalicylic Acid Sodium Salt Dihydrate. *Spectrochim. Acta, Part A* **2002**, *58*, 281−287.
(48) Cintra, E. P.; Córdoba de Torresi, S. I. C.; Errien, N.; Louarn, G. Determination of the Formation of Ladder Structure in Poly(5-amino-1-naphthol) by Resonant Raman and XPS Characterization. *Macromolecules* **2003**, *36*, 2079−2084.
(49) Cao, Q.; Che, R. C.; Chen, N. Scalable Synthesis of Cu_2S Double-Superlattice Nanoparticle Systems with Enhanced UV/Visible-Light-Driven Photocatalytic Activity. *Appl. Catal., B* **2015**, *162*, 187−195.
(50) Mirsaleh-Kohan, N.; Iberi, V.; Simmons, P. D., Jr.; Bigelow, N. W.; Vaschillo, A.; Rowland, M. M.; Best, M. D.; Pennycook, S. J.;

DOI: 10.1021/acsami.5b04769
ACS Appl. Mater. Interfaces 2015, 7, 18491−18500

Masiello, D. J.; Guiton, B. S.; Camden, J. P. Single-Molecule Surface-Enhanced Raman Scattering: Can STEM/EELS Image Electromagnetic Hot Spots? *J. Phys. Chem. Lett.* **2012**, *3*, 2303−2309.
(51) An, Q.; Zhang, P.; Li, J. M.; Ma, W. F.; Guo, J.; Hu, J.; Wang, C. C. Silver-Coated Magnetite−Carbon Core−Shell Microspheres as Substrate-Enhanced SERS Probes for Detection of Trace Persistent Organic Pollutants. *Nanoscale* **2012**, *4*, 5210−5216.
(52) Stamplecoskie, K. G.; Scaiano, J. C.; Tiwari, V. S.; Anis, H. Optimal Size of Silver Nanoparticles for Surface-Enhanced Raman Spectroscopy. *J. Phys. Chem. C* **2011**, *115*, 1403−1409.

DOI: 10.1021/acsami.5b04769
ACS Appl. Mater. Interfaces 2015, 7, 18491−18500